determined by comparison of the conformations obtained by reminimization after systematic variation of the relevant dihedral angles.

X-ray Structural Analysis. Details of the X-ray experimental conditions, cell data, data collection, and refinement procedures for molecule **1** are summarized in Table V. The cell and intensity data were collected with an Enraf-Nonius CAD4 diffractometer using graphite monochromatized Mo Kα radiation. The data were corrected for Lorentz and polarization effects. Intensities of three reflections measured at 2-h intervals showed no sign of decay. Calculations were carried out using the SDP-Plus system of programs and data therein,[15] with SHELX76,[16] and with SHELXS86.[17] The structure was solved by direct methods. Hydrogen atoms bonded to carbon (visible in difference maps) were allowed for (as riding atoms, C-H 0.95 Å). The coordinates for the unique hydroxyl hydrogen were obtained from a difference map (O-H 0.98 Å). Refinement was by least-squares calculations on *F* with all non-H atoms allowed anisotropic motion. All phenyl and pyridine rings were constrained to be rigid hexagons with standard bond lengths. The decision as to which was a nitrogen atom and which was a carbon in the pyridine rings was unequivocally made from difference maps (by the unambiguous location of all pyridine H atoms). Selected dimensions are in Table III. Figures 5 and 6 were prepared with the aid of ORTEPII[18] and PLUTON[19] programs.

Additional material available from the Cambridge Crystallographic Data Centre comprises atom coordinates, thermal parameters, and a full listing of bond lengths and angles for **1**. Copies of the structure factor listings are available from the authors.

Acknowledgment. Italian authors thank M.U.R.S.T. for partial financial support of this work. G.F. thanks NSERC Canada for grants in aid of research. M.P. acknowledges support by Grant PB89-257 from DGICYT. M.A.M. holds a predoctoral grant from Farmhispania.

Registry No. 1, 139378-46-4; *p-tert*-butylcalix[6]arene, 78092-53-2; 2-picolyl chloride hydrochloride, 6959-47-3.

Supplementary Material Available: Tables listing final fractional coordinates for all non-H atoms, calculated hydrogen coordinates, molecular dimensions, anisotropic thermal parameters, mean plane data, and selected torsion angles (10 pages); tables listing structure factors for **1** (6 pages). Ordering information is given on any current masthead page.

(15) SDP-Plus Program system, B. A. Frenz and Associates, Inc., College Station, TX, and Enraf-Nonius, Delft, Holland, 1983.
(16) Sheldrick, G. M. SHELX76. A Program for Crystal Structure Determination. University of Cambridge, England, 1976.
(17) Sheldrick, G. M. *SHELXS86. Crystallographic computing 3*; Sheldrick, G. M., Kruger, C., Goddard, R., Eds.; Oxford Univ. Press: London, 1986; pp 175-189.
(18) Johnson, C. K. ORTEPII. Report ORNL-5138; Oak Ridge National Laboratory: Oak Ridge, TN, 1976.
(19) Spek, A. L. PLUTON. Molecular Graphics Program. University of Utrecht, The Netherlands, 1991.

Influence of Solute-Fluid Clustering on the Photophysics of Pyrene Emission in Supercritical C_2H_4 and CF_3H

JoAnn Zagrobelny and Frank V. Bright*

Contribution from the Department of Chemistry, Acheson Hall, State University of New York at Buffalo, Buffalo, New York 14214. *Received April 23, 1992*

Abstract: In this paper, we continue our investigations of the photophysics of pyrene emission in supercritical fluids using steady-state and time-resolved fluorescence spectroscopy. Specifically, we study pyrene photophysics in sub- and supercritical C_2H_4 and CF_3H. Steady-state fluorescence is utilized to determine how the local fluid density affects the ground and excited states of pyrene and to probe any potential ground-state dimerization (preassociation). Time-resolved fluorescence provides details of the mechanism of pyrene excimer formation and the kinetics of solute-solute interactions. The temperature and density dependence of the recovered bimolecular rate constant for pyrene in supercritical C_2H_4 follows that which had been reported in supercritical CO_2 and liquid solvents, i.e., the excimer formation is diffusion controlled. In supercritical CF_3H, this rate constant is much slower than predicted based on diffusion control arguments. These results indicate that enhanced solute-solvent interactions (clustering) strongly affect the pyrene excimer reaction in CF_3H.

Introduction

The characteristic critical point for any chemical species is defined by its critical temperature and pressure. Immediately below these points there exists an equilibrium between the liquid and gaseous phases. However, once the critical point is reached, the two phases coalesce into one known as a supercritical fluid. In this region the physicochemical properties, e.g., density, diffusivity, viscosity, and dielectric constant, can be continuously adjusted without passing through a phase boundary, and the inherent molecular structure of the solvent is maintained.[1-4] Thus, supercritical fluids can be considered a continuously tunable (with pressure and temperature or density) solvent system.

Because of their unique tunability, supercritical fluids have been used in a number of scientific research areas.[1-18] For example, extractions,[2-5] chromatography,[6-9] and chemical reactions[14] are all routinely carried out in supercritical solvents. However, in spite of their widespread use in science and technology, we do not yet completely understand how supercritical fluids behave compared to liquids and gases. Specifically, we do not fully understand

* Author to whom all correspondence should be addressed.

(1) Reid, R. C.; Prausnitz, J. M.; Poling, B. E. *The Properties of Gases and Liquids*, 4th ed.; McGraw Hill: New York, 1987.
(2) Bruno, T. J.; Ely, J. F. *Supercritical Fluid Technology: Reviews in Modern Theory and Applications*; CRC Press: Boca Raton, FL, 1991.
(3) Paulaitis, M. E.; Krukonis, V. J.; Kurnik, R. T.; Reid, R. C. *Rev. Chem. Eng.* **1983**, *1*, 179.
(4) Paulitis, M. E.; Kander, R. G.; DiAndreth, J. R. *Ber. Bunsen-Ges. Phys. Chem.* **1984**, *88*, 869.
(5) Brennecke, J. F.; Eckert, C. A. *AIChE J.* **1989**, *35*, 1409.
(6) Klesper, E. *Angew. Chem., Int. Ed. Engl.* **1978**, *17*, 738.
(7) Novotny, M. V.; Springston, S. R.; Peaden, P. A.; Fjeldsted, J. C.; Lee, M. L. *Anal. Chem.* **1981**, *53*, 407A.
(8) *Supercritical Fluid Chromatography*; Smith, R. M., Ed.; Royal Society of Chemistry Monograph; Royal Society of Chemistry: London, UK, 1988.
(9) Smith, R. D.; Wright, B. W.; Yonker, C. R. *Anal. Chem.* **1988**, *60*, 1323A.
(10) Brunner, G. *Ion. Exch. Solvent Extr.* **1988**, *10*, 105.
(11) Eckert, C. A.; Van Alsten, J. G. *Environ. Sci. Technol.* **1986**, *20*, 319.

0002-7863/92/1514-7821$03.00/0

how supercritical solvents can affect chemical reactions.

Eckert and co-workers[19,20] were the first to show that the partial molar volume for solutes at infinite dilution was large and negative near the fluid critical point. This result indicated (in a macroscopic sense) that when solute was added to the fluid medium that the fluid tended to collapse or cluster about the solute. Following this initial observation, many research groups have investigated the interactions between solvent clusters and solute molecules. For example, Johnston et al.[21-25] have used spectroscopic techniques to show that the local density in the cybotactic region about the solute can be significantly greater than the bulk fluid density. In these experiments, local densities were recovered by comparing the observed spectral shifts with expected values based on the linear McRae continuum model.[26,27] A model based on Kirkwood-Buff solution theory sufficed to describe the spectral data. Yonker, Smith, and co-workers[28] also reported deviations from the McRae continuum model and attributed this qualitatively to solute-fluid clustering.

Steady-state fluorescence spectroscopy has been used by the Okada[29] and Kajimoto[30] groups to study intramolecular excited-state complexation and charge-transfer formation in supercritical fluids. Once again, the observed spectral shifts were greater than predicted by theory and were attributed to solute-fluid clustering. Our own group has combined steady-state and time-resolved fluorescence spectroscopy to show that there is a distribution of cluster domains surrounding the solute.[31,32] Most recently, we have used fluorescence anisotropy and lifetime measurements to determine the actual cluster size.[33]

Brennecke and Eckert used the fluorescent solute pyrene to probe the clustering process in supercritical CO_2, C_2H_4, and CF_3H.[5,34-36] Changes in the environmentally-sensitive vibronic bands of the pyrene emission, as a function of fluid density, were used to measure the extent of solute-fluid interaction and cluster formation. Additional studies of the pyrene excimer were consistent with enhanced solute-solute interactions in supercritical fluids.[5,34-36] In these experiments, the authors reported pyrene excimer-like emission at much lower concentrations than is required to observe the excimer in liquids (μM concentration in supercritical fluids versus mM in liquids).

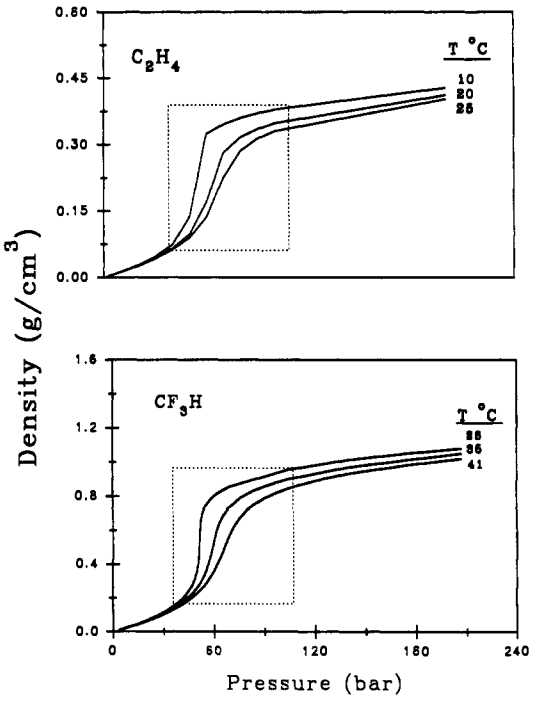

Figure 1. Density-pressure isotherms showing the region (boxed area) over which experiments were carried out in C_2H_4 and CF_3H.

In related studies, Kurnik and Reid[37] and Kwiatkowski et al.[38] observed synergistic effects on the solubilities of mixed solutes in supercritical solvents. That is, the solubilities of two components were greater than the solubilities of the individual component in the same fluid. In normal liquids, one does not observe such synergism. These results suggest that solute-solute interactions affect solute-fluid chemistry in the supercritical region. This further suggests that solute-solute interactions are much stronger in supercritical fluids versus liquid media and can affect predicted phase behavior.

In an effort to improve our understanding of solute-solute interactions in supercritical fluids, our group investigated in detail the photophysics of pyrene in supercritical CO_2.[39] By using steady-state *and* time-resolved fluorescence spectroscopy, we were able to determine how solute-solute interactions are affected by supercritical CO_2. The results of these experiments showed clearly that (1) pyrene excimer formation follows the same mechanism as seen in liquids (i.e., the reaction is completely diffusion controlled), (2) pyrene excimer is observed in supercritical fluids at much lower concentrations than is necessary in liquids because of the increased diffusivity, and (3) solute-fluid clustering did not lead to any enhanced interaction of ground-state pyrene species (i.e., there was no preassociation).

The current research expands on our earlier work by investigating the photophysics of pyrene in sub- and supercritical CF_3H and C_2H_4. In this work we focus on determining how different

(12) *Supercritical Fluids-Chemical Engineering Principles and Applications*; Squires, T. G., Paulitis, M. E., Eds.; ACS Symposium Series 329; American Chemial Society: Washington, DC, 1987.
(13) van Wasen, I.; Swaid, I.; Schneider, G. M. *Angew. Chem., Int. Ed. Engl.* **1980**, *19*, 575.
(14) Aaltonen, O.; Rantakyla, M. *CHEMTECH* **1991**, *21*, 240.
(15) Bright, F. V.; McNally, M. E. *Recent Advances in Supercritical Fluid Technology: Theoretical and Applied Approaches to Analytical Chemistry*; Bright, F. V., McNally, M. E., Eds.; ACS Symposium Series 488; American Chemical Society: Washington, DC, 1992.
(16) Onuska, F. I.; Terry, K. A. *HRC & CC, J. High Resolut. Chromatogr. Chromatogr. Commun.* **1989**, *12*, 357.
(17) McNally, M. E.; Wheeler, J. R. *J. Chromatogr.* **1988**, *447*, 53.
(18) Onuska, F. I.; Terry, K. A. *HRC & CC, J. High Resolut. Chromatogr. Chromatogr. Commun.* **1989**, *12*, 527.
(19) Eckert, C. A.; Ziger, D. H.; Johnston, K. P.; Ellison, T. K. *Fluid Phase Equilib.* **1983**, *14*, 167.
(20) Eckert, C. A.; Ziger, D. H.; Johnston, K. P.; Kim, S. *J. Phys. Chem.* **1986**, *90*, 2738.
(21) Kim, S.; Johnston, K. P. *Ind. Eng. Chem. Res.* **1987**, *26*, 1206.
(22) Kim, S.; Johnston, K. P. *AIChE J.* **1987**, *33*, 1603.
(23) Johnston, K. P.; Kim, S.; Combs, J. In *Proceedings of the International Symposium on Supercritical Fluids*, Nice, France; Perrut, M., Ed.; 1988; p 263.
(24) Johnston, K. P.; Kim, S.; Wong, J. M. *Fluid Phase Equilib.* **1987**, *38*, 39.
(25) Hrnjez, B. J.; Yazdi, P. T.; Fox, M. A.; Johnston, K. P. *J. Am. Chem. Soc.* **1989**, *111*, 1915.
(26) Bayliss, N. S.; McRae, E. G. *J. Phys. Chem.* **1954**, *58*, 1002.
(27) McRae, E. G. *J. Phys. Chem.* **1957**, *61*, 562.
(28) Yonker, C. R.; Frye, S. L.; Kalkwarf, D. R.; Smith, R. D. *J. Phys. Chem.* **1986**, *90*, 3022.
(29) Okada, T.; Kobayashi, Y.; Yamasa, H.; Mataga, N. *Chem. Phys. Lett.* **1986**, *128*, 583.
(30) Kajimoto, O.; Futakami, M.; Kobayashi, T.; Yamasaki, K. J. *J. Phys. Chem.* **1988**, *92*, 1347.
(31) Betts, T. A.; Zagrobelny, J.; Bright, F. V. *J. Supercrit. Fluids* **1992**, *5*, 48.
(32) Betts, T. A.; Zagrobelny, J.; Bright, F. V. In *Recent Advances in Supercritical Fluid Technology: Theoretical and Applied Approaches to Analytical Chemistry*; Bright, F. V., McNally, M. E., Eds.; ACS Symposium Series 488; American Chemical Society: Washington, DC, 1992, Chapter 4.
(33) Betts, T. A.; Zagrobelny, J.; Bright, F. V. *J. Am. Chem. Soc.*, in press.
(34) Brennecke, J. F.; Eckert, C. A. In *Supercritical Fluid Science and Technology*; Johnston, K. P., Penninger, J. M. L., Eds.; ACS Symposium *Series* 406; American Chemical Society: Washington, DC, 1989, Chapter 2.
(35) Brennecke, J. F.; Tomasko, D. L.; Peshkin, J.; Eckert, C. A. *Ind. Eng. Chem. Res.* **1990**, *29*, 1682.
(36) Brennecke, J. F.; Tomasko, D. L.; Eckert, C. A. *J. Phys. Chem.* **1990**, *94*, 7692.
(37) Kurnik, R. T.; Reid, R. C. *Fluid Phase Equilib.* **1982**, *8*, 93.
(38) Kwiatkowski, J.; Lisicki, Z.; Majewski, W. *Ber. Bunsen-Ges. Phys. Chem.* **1984**, *88*, 865.
(39) Zagrobelny, J.; Betts, T. A.; Bright, F. V. *J. Am. Chem. Soc.* **1992**, *114*, 5249.

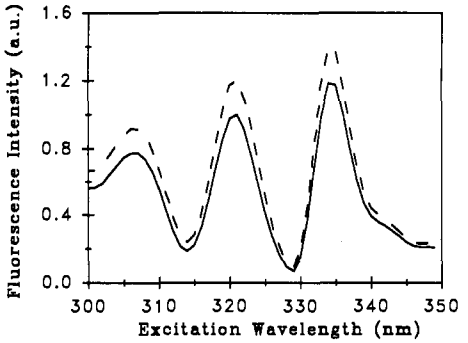

Figure 2. Normalized, emission wavelength-dependent steady-state excitation spectra of 100 μM pyrene in supercritical C_2H_4 at 12.5 °C and a reduced density of 1.03. The solid line is the spectrum for the monomer (λ_{em} = 380 nm) and the long, dashed line is for the dimer (if present) (λ_{em} = 460 nm). Excitation spectral bandpass = 2 nm. Emission spectral bandpass = 16 nm. The entire monomer spectrum is purposefully offset for clarity.

supercritical fluids affect the kinetics of pyrene excimer formation. With these new results we are able to systematically compare and contrast the effects of CO_2,[39] C_2H_4, and CF_3H on the pyrene excimer formation reaction.

Experimental Section

Detailed information on the experimental apparatus and instrumentation can be found in our earlier paper.[39] All steady-state fluorescence experiments were carried out using a SLM 48000 MHF spectrofluorometer (SLM Instruments) modified to accommodate the high-pressure optical cells.[39-41] A 450-W Xe-arc lamp serves as the excitation source, and monochromators are used for excitation and emission wavelength selection.

All time-resolved experiments were carried out using an in-house-constructed N_2 laser/boxcar-based system interfaced to a personal computer.[39] The control/acquisition BASIC software was developed and written in our laboratory. The time-resolved intensity decay data are analyzed using a commercially available software package (Globals Unlimited, Urbana, IL).

CF_3H (98%) and CP grade C_2H_4 were purchased from Scott Specialty Gases. Prior to entering the pump system, each was passed through an oxygen trap, an activated carbon column (Matheson), and a 0.2-μm filter. Pyrene was obtained from Aldrich (99%) and used as received after checking its purity by reverse-phase HPLC (C_{18}). Stock solutions of pyrene were prepared in absolute ethanol (Quantum). An aliquot from the stock pyrene solution (1 mM) is micropipetted directly into the optical cell, and the cell is charged as described previously.[39]

All C_2H_4 and CF_3H experiments were conducted in the highly compressible region closest the critical point (Figure 1).

Results and Discussion

Steady-State Experiments. The very first issue we were concerned with was the presence of any fluid-induced pyrene–pyrene preassociation in the ground state. To address this concern, we acquired a large series of emission wavelength-dependent steady-state excitation spectra as a function of C_2H_4 and CF_3H density and temperature.[39] A typical set of these spectra for 100 μM pyrene in C_2H_4 (T_r = 1.01) and CF_3H (T_r = 1.03) are shown in Figures 2 and 3, respectively. In each case, the reduced density was very near the critical density. Clearly, the shape of the excitation contours are essentially identical at the two emitting wavelengths. This result is consistent with only a single species being present in the ground state (i.e., no pyrene–pyrene dimer is formed in the ground state). Similar spectral contours are observed for all temperatures and densities studied, showing that temperature and pressure do not affect the spectra. This behavior is similar to our observations in supercritical CO_2.[39]

For completeness, Figure 4 shows the recovered correlation coefficients for the entire set of intensity–intensity correlation plots.[39] To generate this data, the individual emission wavelength-dependent excitation spectra are first normalized at their

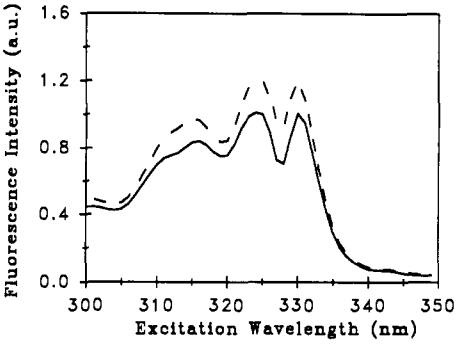

Figure 3. Normalized, emission wavelength-dependent steady-state excitation spectra of 100 μM pyrene in supercritical CF_3H at 30 °C and a reduced density of 1.01. Same symbolism and protocol as in Figure 2.

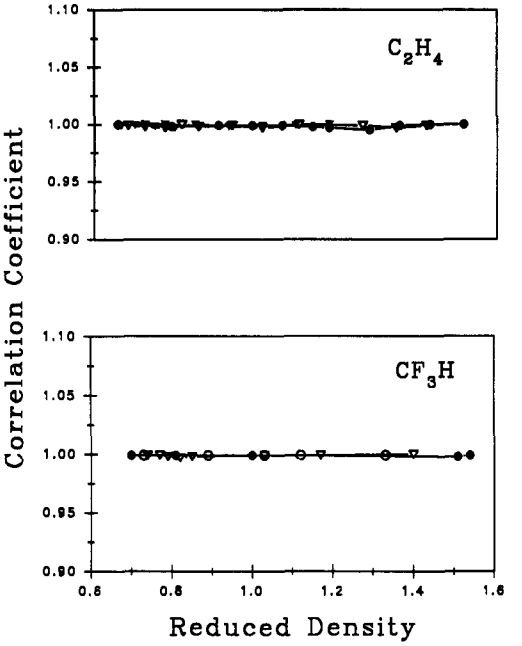

Figure 4. Recovered correlation coefficients for correlation plots (monomer intensity versus excimer intensity) as a function of fluid temperature and reduced density. (symbol, T_r): C_2H_4, (●, 1.01); (▽, 1.03); (▼, 1.05); CF_3H, (○, 1.01); (●, 1.03); (▽, 1.05).

peak maxima, and then the intensity of the "excimer" scan (λ_{em} = 460 nm) is plotted versus the intensity of the "monomer" (λ_{em} = 380 nm). If the pyrene spectral contours overlap completely, i.e., the ground state is homogeneous, one would obtain a straight line with a slope of unity, an intercept of zero and a correlation coefficient of one.[39] Inspection of the results in Figure 4 shows that there is no evidence of pyrene–pyrene preassociation at any temperature/density combination.

The excitation spectrum of pyrene in C_2H_4 is similar to that observed in CO_2.[39] However, the excitation spectrum in CF_3H is quite different. For the long-wavelength band a hypsochromic shift is seen, and for the shorter wavelength band a bathochromic shift is observed indicating a more polar environment. This is caused by the more polar CF_3H fluid stabilizing the nonbonding molecular orbital and destabilizing the π molecular orbital. Therefore, the long-wavelength band ($n \rightarrow \pi^*$) increases in energy (blue shift) and the short-wavelength band ($\pi \rightarrow \pi^*$) decreases in energy (red shift). This type of solvent effect on the absorption spectra of organic molecules has been thoroughly investigated by Burawoy.[42]

Typical density-dependent emission spectra for 100 μM pyrene in sub- and supercritical C_2H_4 and CF_3H, T_r = 1.01, are shown in Figure 5. Clearly, the fluid density affects strongly the amount

(40) Betts, T. A.; Bright, F. V. *Appl. Spectrosc.* **1990**, *44*, 1196.
(41) Betts, T. A.; Bright, F. V. *Appl. Spectrosc.* **1990**, *44*, 1204.
(42) Burawoy, A. *J. Chem. Soc.* **1939**, 1177.

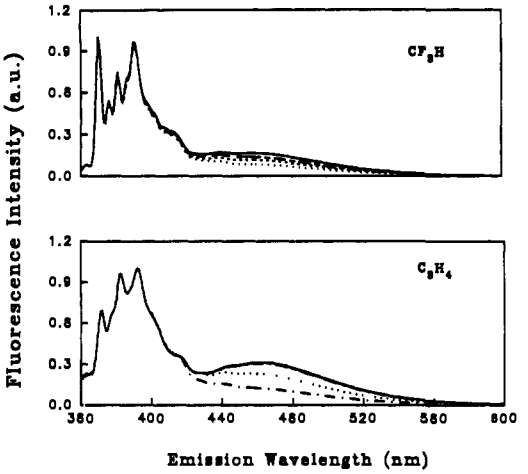

Figure 5. Steady-state emission spectra for 100 μM pyrene in sub- and supercritical CF_3H (upper panel) and sub- and supercritical C_2H_4 (lower panel) as a function of density at reduced temperatures of 1.01 and 1.03, respectively. λ_{ex} = 337 nm. Excitation spectral bandpass = 16 nm. Emission spectral bandpass = 2 nm. In both panels, the excimer emission is decreasing with increasing density (ρ_r = 0.85 → 1.85).

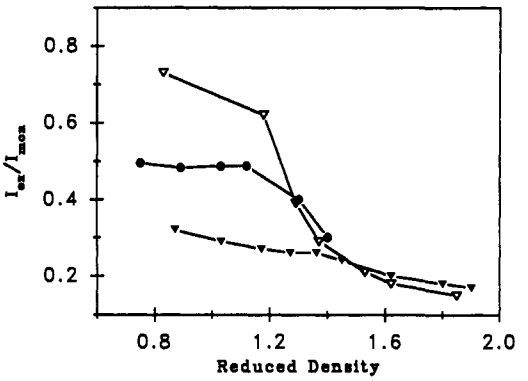

Figure 6. Monomer-to-excimer intensity ratio for 100 μM pyrene in supercritical fluids as a function of density. (symbol, fluid, T_r): (▽, CO_2, T_r = 1.00); (●, C_2H_4, T_r = 1.01); (▼, CF_3H, T_r = 1.01).

of excimer formed. As the density increases, the relative amount of excimer emission decreases. Further, the amount of excimer formed in CF_3H is much less than that in either CO_2[39] or C_2H_4. This is more clearly illustrated in Figure 6 which shows the excimer-to-monomer intensity ratio (I_{ex}/I_{mon}) as a function of reduced density. The intensities of the monomer and excimer are recovered by determining the area, by integration, in the regions 367–420 and 440–500 nm, respectively.

Close inspection of the emission spectra also show that the ratio of the first vibronic band to the third vibronic band (I_1/I_3) is much larger in CF_3H than C_2H_4, which indicates stronger solute–fluid interaction (Figure 7). The intensity of the O–O transition (I_1) is solvent dependent[43-45] and increases with solute–solvent interaction. In contrast, the I_3 transition is solvent independent. Thus, the I_1/I_3 ratio is a convenient measure of the extent of solute–solvent interactions, and the value of the ratio increases as interactions increase. The large ratio was also observed by Brennecke, et al.[36] who used it to measure the extent of solvent clustering in CO_2, C_2H_4, and CF_3H.

Although the steady-state results provide key insights into the system photophysics, they are incomplete. To fully understand how the supercritical solvent affects the pyrene excimer reaction it is necessary to use time-resolved fluorescence spectroscopy.[39]

Time-Resolved Experiments. From our steady-state results (Figures 2–4) we found that the pyrene ground state is homo-

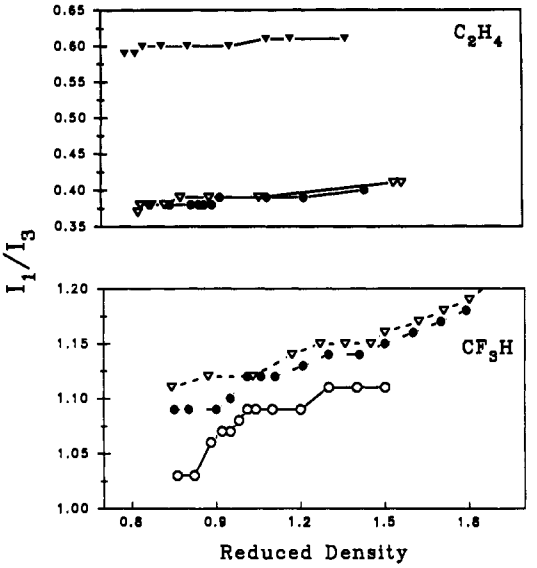

Figure 7. Ratio of the intensity of the first vibronic peak (I_1, 367–374 nm) to the third vibronic peak (I_3, 379–384 nm) for pyrene in supercritical C_2H_4 and CF_3H as a function of reduced density. (symbol, T_r): C_2H_4, (▼, 1.01); (▽, 1.03); (●, 1.05); CF_3H, (▽, 1.00); (●, 1.03); (○, 1.05).

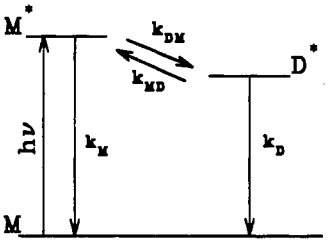

Figure 8. Energy-level diagram for pyrene excimer formation in supercritical fluids. Symbols represent the following: $h\nu$, absorbed photon, k_M, decay rate for monomer; k_{DM}, bimolecular rate coefficient for excimer formation; k_{MD}, unimolecular rate coefficient for dissociation of excimer; k_D, decay rate for excimer; M*, excited-state monomer; and D*, excited-state dimer (excimer). Note: No ground-state preassociation is indicated.

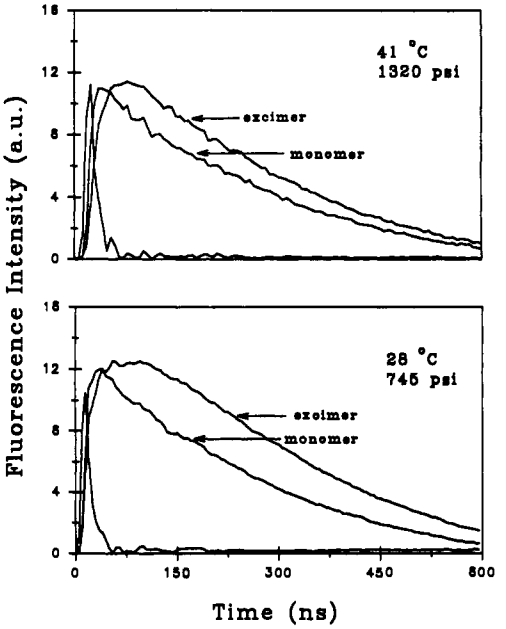

Figure 9. Typical time-resolved fluorescence decay traces for pyrene in supercritical CF_3H at 28 °C, P = 745 psi; lower panel and 41 °C, P = 1320 psi; upper panel.

geneous at all densities and temperatures studied. Thus, we know that our excited-state decay kinetics follow the classical excimer

(43) Dong, D. C.; Winnik, M. A. *Can. J. Chem.* **1984**, *62*, 2560.
(44) Dong, D. C.; Winnik, M. A. *Photochem. Photobiol.* **1982**, *35*, 17.
(45) Ham, J. S. *J. Chem. Phys.* **1953**, *21*, 756.

Table I. Comparison of Experimentally Recovered and Theoretical Values for the Forward Bimolecular Rate Coefficient (k_{DM}) for Pyrene Excimer Formation in Sub- and Supercritical CF_3H

T (°C)	P (bar)	$k_{DM} \times 10^{11}$ (M^{-1} s^{-1}) expt[a]	$k_{DM} \times 10^{11}$ (M^{-1} s^{-1}) theor[b]
28	51.0	0.08	2.2
	51.4	0.10	2.1
	54.8	0.19	1.7
	58.9	0.21	1.6
35	58.6	0.08	2.4
	60.0	0.08	2.2
	69.3	0.19	1.7
	75.8	0.24	1.6
41	64.8	0.35	2.6
	67.6	0.21	2.4
	82.0	1.6	1.7
	91.0	1.7	1.6

[a] Experiments were performed by maintaining the corresponding temperature and adjusting the pressure. Fluorescence decays were obtained at three different wavelengths for two different pyrene concentrations. The rate coefficients were recovered by linking the spectral contours over the entire multidimensional data surface.[39] The uncertainties in recovered rates are ≤10%. [b] Calculated from $k_{DM} = 8000RT/0.3\eta$.[53]

Table II. Comparison of Experimentally Recovered and Theoretical Values for the Forward Bimolecular Rate Coefficient (k_{DM}) for Pyrene Excimer Formation in Sub- and Supercritical C_2H_4

T (°C)	P (bar)	$k_{DM} \times 10^{11}$ (M^{-1} s^{-1}) expt[a]	$k_{DM} \times 10^{11}$ (M^{-1} s^{-1}) theor[b]
10	50.7	3.6	3.7
	51.0	3.6	3.6
	57.7	1.6	2.0
	60.3	1.6	1.7
20	68.6	3.6	2.3
	69.4	2.7	2.3
	81.7	2.6	1.8
	90.3	2.3	1.7
25	69.1	3.7	3.0
	70.3	2.9	2.9
	82.7	2.1	2.1
	96.5	1.7	1.8

[a] Experiments were performed by maintaining the corresponding temperature and adjusting the pressure. Fluorescence decays were obtained at three different wavelengths for two different pyrene concentrations. The rate coefficients were recovered by linking the spectral contours over the entire multidimensional data surface.[39] The uncertainties in recovered rates are ≤10%. [b] Calculated from $k_{DM} = 8000RT/0.3\eta$.[53]

decay model (Figure 8), and the associated rates can be recovered by simultaneous global analysis of multiple fluorescence decay experiments.[39,46-51]

Figure 9 shows a typical set of decay traces for 100 μM pyrene in supercritical CF_3H. The lower and upper panels illustrate the decay traces for the monomer (400 nm) and the excimer (450 nm) emissions at conditions close to and far from the critical point, respectively. Full, global analysis of this data[39,46-51] yields values of the individual rate terms (Figure 8) for the pyrene excimer photophysics. The entire ensemble of recovered rates are collected in Tables I–IV and show some intriguing trends.

Table III. Experimentally Recovered Values for the Reverse Unimolecular Rate Coefficient (k_{MD}) and Emissive Decay Rates For the Monomer (k_M) and Excimer (k_D) in Sub- and Supercritical CF_3H[a]

T (°C)	P (bar)	$k_{MD} \times 10^7$ (s^{-1})	$k_M \times 10^6$ (s^{-1})	$k_D \times 10^8$ (s^{-1})
28	51.0	4.6×10^{-4}	2.7	0.34
	51.4	0.88	2.7	0.73
	54.8	1.3	2.7	0.59
	58.9	6.7	1.5	0.59
35	58.6	0.29	2.9	0.30
	60.0	0.59	2.5	0.49
	69.3	1.6	1.6	0.62
	75.8	2.6	2.1	1.1
41	64.8	4.0	2.5	0.73
	67.6	2.0	2.5	4.4
	82.0	1.5×10^3	2.6	22
	91.0	1.3×10^3	2.5	20

[a] Same experimental procedure as described in footnote *a* of Table I. The uncertainties in recovered rates are ≤10%.

Table IV. Experimentally Recovered Values for the Reverse Unimolecular Rate Coefficient (k_{MD}) and Emissive Decay Rates for the Monomer (k_M) and Excimer (k_D) in Sub- and Supercritical C_2H_4[a]

T (°C)	P (bar)	$k_{MD} \times 10^{10}$ (s^{-1})	$k_M \times 10^6$ (s^{-1})	$k_D \times 10^8$ (s^{-1})
10	50.7	1.9	2.2	1.8×10^{-3}
	51.0	1.8	2.1	3.8×10^{-3}
	57.7	1.7	2.1	0.67
	60.3	1.7	2.1	8.8
20	68.6	1.5	2.4	6.4
	69.4	1.5	2.1	5.3
	81.7	1.5	2.1	6.9
	90.3	1.3	2.1	15
25	69.1	1.7	2.5	23
	70.3	1.6	2.5	23
	82.7	1.7	2.5	37
	96.5	1.6	2.2	45

[a] Same experimental procedure as described in footnote *a* of Table I. The uncertainties in recovered rates are ≤10%.

Near the critical point, the recovered forward bimolecular rate (k_{DM}) for pyrene excimer formation in CF_3H is significantly less than the rate predicted based on diffusion control. However, at higher temperatures and pressures, where there is less solute–fluid clustering,[5,19-36] the excimer formation rate becomes diffusion controlled. This is in contrast to C_2H_4 (Table II) and CO_2,[39] where the excimer formation is completely diffusion controlled for all temperatures and pressures near and far from the critical point. (The viscosities needed to calculate the theoretical diffusion-controlled rate constant[39] in C_2H_4 were obtained by plotting the literature values[52] and interpolating for the specific experimental conditions. Viscosities for CF_3H were estimated based on the Reichenberg equation of state.[1])

The remaining photophysical rate parameters (Figure 8) are collected in Tables III and IV for pyrene in CF_3H and C_2H_4, respectively. The unimolecular dissociation rate constant (k_{MD}) for pyrene excimer formation changes such that the apparent equilibrium constant ($K_{eq\,app} = k_{DM}/k_{MD}$) decreases with increasing fluid density. The magnitude of k_{MD} in CF_3H is much smaller than the values recovered in C_2H_4 and CO_2,[39] which leads to a substantial increase in $K_{eq\,app}$ for CF_3H. From this piece of information alone, one would predict that there would be greater levels of excimer emission (relative to the monomer) in CF_3H compared to C_2H_4 or CO_2. Of course, one must realize that k_{DM} in CF_3H is much slower than that predicted by diffusion control, which indicates that once the excimer complex forms it is most "stable" in CF_3H; however, it is precluded from forming due to solvent clustering about the pyrene species. Thus, although the excimer complex is most stable in CF_3H, we observe less excimer

(46) Beecham, J. M.; Gratton, E. In *Time-Resolved Laser Spectroscopy in Biochemistry*; Lakowicz, J. R., Ed.; *Proc. SPIE, Int. Soc. Opt. Eng.* **1988**, *909*, 70.
(47) Beecham, J. M.; Ameloot, M.; Brand, L. *Chem. Phys. Lett.* **1985**, *120*, 466.
(48) Beecham, J. M.; Ameloot, M.; Brand, L. *Anal. Instrum.* **1985**, *14*, 379.
(49) Huang, J.; Bright, F. V. *J. Phys. Chem.* **1990**, *94*, 8457.
(50) Ameloot, M.; Boens, N.; Andriessen, R.; Van der Bergh, V.; De Schryver, F. C. *J. Phys. Chem.* **1991**, *95*, 2047.
(51) Andriessen, R.; Boens, N.; Ameloot, M.; De Schryver, F. C. *J. Phys. Chem.* **1991**, *95*, 2047.
(52) *Gas Encyclopedia* **1976**, 483.

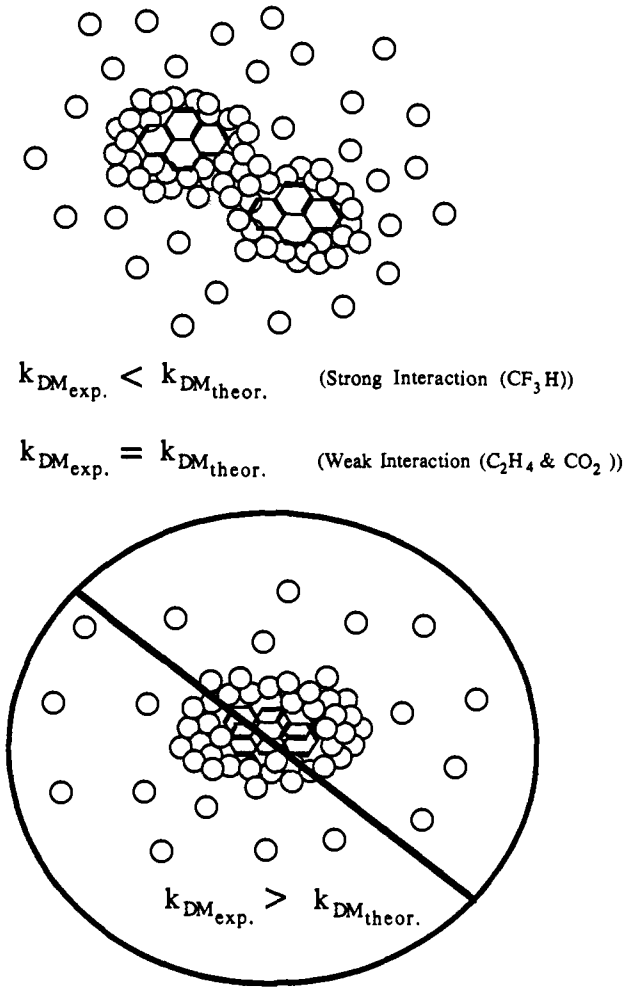

Figure 10. Summary of the type of pyrene–fluid interactions seen in supercritical solvents. The upper portion summarizes the results for CF_3H, CO_2, and C_2H_4. It shows that clustering does occur, but does not influence the excimer formation process in CO_2 and C_2H_4. Clustering does affect the excimer formation in CF_3H. The lower section shows that ground-state solute–solute interactions are not a manifestation of the clustering process. k_{DM} denotes the forward bimolecular rate term. The subscripts exp. and theor. present the recovered and predicted (based on diffusion control) rates, respectively.

(Figure 5) as a consequence of clustering.

For pyrene in C_2H_4 we observe the same behavior for the excimer decay rate, k_D, as we saw in CO_2.[39] The value for k_D is smallest near the critical point and increases as we move from the region of highest compressibility. Again, we find that the fluid does not affect how the excimer is formed. However, once it has formed there is association between the cluster and the excimer, such that the excimer is stabilized and shielded from nonradiative decay. Although we see the same type of trend in CF_3H at higher temperatures, this rate remains relatively constant when there are enhanced interactions with the solvent cluster and the monomer. Further, this rate is faster in CF_3H than that in either C_2H_4 or CO_2, which indicates that the CF_3H cluster is not as effective at protecting the excimer from quenching effects.

For all fluids investigated the emissive decay rate for pyrene monomer (k_M) is unaffected by temperature and pressure and is of the same magnitude as that in liquids.[53]

Conclusions

In an effort to compare and contrast the effect of various supercritical fluids on chemical reactions, we have performed a detailed analysis of the photophysics of pyrene in sub- and supercritical C_2H_4 and CF_3H. This work, which expands on our previous report,[39] shows that these supercritical fluids affect the pyrene excimer reaction differently (Figure 10). By comparing the photophysics of pyrene excimer emission in CO_2, C_2H_4, and CF_3H, we find that CO_2 and C_2H_4 behave similarly. That is, the solute–fluid cluster, which forms in the region near the critical point,[5,34-36] does not affect the formation of excimer, and the reaction is completely diffusion controlled. It does occur on a faster time scale than the same reaction in liquids,[53] but only because of the increased diffusivity in supercritical fluids. Once the excimer is formed there are enhanced interactions between the solvent cluster and the excimer. This is indicated by a substantial increase in the emissive decay rate at higher temperatures and pressures, showing that clustering may protect the excimer from quenching effects.

In contrast, the excimer formation reaction in CF_3H proceeds more slowly than predicted by diffusion control. These results indicate that the CF_3H cluster interacts much more strongly with the pyrene molecules such that they impede excimer formation. Interestingly, we find that once the excimer is formed, the CF_3H apparently cannot shield it as well as the other fluids. Perhaps the cluster sizes of CO_2 and C_2H_4 are larger than CF_3H and provide a more protective environment for the formed pyrene excimer. Alternatively, it may be possible that the cluster cannot rearrange itself enough to accommodate the entire excimer species on the nanosecond time scale of the excimer reaction.

From this work we also conclude that there is no ground-state association of pyrene molecules in any of the supercritical fluids studied. Apparently, the solute–fluid clusters are not strong enough to overcome the inherent repulsive nature of ground-state pyrene species.[53] Even the enhanced interactions of pyrene in supercritical CF_3H are not great enough to force solute–solute interactions to occur prior to excitation. Again, if there were any indication of ground-state interaction we would have seen it by our emission wavelength-dependent excitation scans (Figures 2 and 3), and there would have been an increase in the rate k_{DM} expected for diffusion control. This is not the case.

We find that pyrene excimer observed at micromolar concentrations in supercritical CO_2 and C_2H_4 is due to the following: (1) the increased diffusivity and (2) fluid–excimer interactions where CO_2 acts to stabilize the excimer excited state. Thus, CO_2 and C_2H_4 clusters do not affect the mechanism of excimer formation; however, once the excimer forms these fluids affect the excimer decay rate. In contrast, pyrene excimer formation occurs in CF_3H because the apparent excited-state equilibrium constant favors excimer formation. However, the forward reaction is appreciably slowed (vide supra). These interactions are stronger for CF_3H clusters and the pyrene monomer, but are weaker for the excimer, i.e., the emissive decay rate is greater in CF_3H than that in either CO_2 or C_2H_4. These conclusions are summarized in Figure 10.

Acknowledgment. This work has been generously supported by the United States Department of Energy (DE-FGO2-920ER14143).

Registry No. C_2H_4, 74-85-1; CF_3H, 75-46-7; pyrene, 129-00-0.

(53) Birks, J. B.; Dyson, D. J.; Munro, I. H. *Proc. Roy. Soc. A* **1963**, *275*, 575.